DAΦNE TECHNICAL NOTE

INFN - LNF, Accelerator Division

CALIBRATION CONSTANTS AND NOMINAL SET POINTS FOR THE DAY-ONE LATTICE OF THE DAΦNE MAIN RINGS

S. Guiducci, M. Preger

Introduction

This Technical Note aims at summarizing in few simple formulas the results of the magnetic measurements on the magnets of the DAΦNE Main Rings concerning the constants and nominal values to be introduced in the DataBase of the Control System.

The magnets are subdivided into different groups, which collect the data corresponding to magnets of the same type. A paragraph is dedicated to each one of such groups, where the calibration constants relating the excitation current to the physical characteristics of the magnet are given. Where necessary, a brief discussion of the limits on the accuracy of the calibration is recalled, with reference to the original Technical Notes for further improvements of the Control System capabilities. Within each group the single magnets are collected into Tables, showing the nominal set points of the DAY-ONE lattice, as given in [1]. These Tables show, in addition, the correspondence between the standard names of the magnets [2] and the serial numbers presented in all the Technical Notes dedicated to the magnetic measurements results.

The sequence followed in the Tables follows the path of the particles in the two rings as shown in Figure 1. The first half starts from the injection point in the **e⁻** ring, going trough sections *EL1, IR1(KLOE), ES1, ES2, IR2 (FINUDA),* and *EL2* in the counterclockwise direction (looking at the rings from above). The second half follows the **e⁺** ring in the same way, obviously in the clockwise direction. The magnets in the region shared by the two beams *(IRs)* are mentioned only in the first loop in the direction of the **e⁻**. A blank row separates the **e⁻** loop from the **e⁺** one where the two loops are not shown in different columns.

The data presented in this Note are restricted to the nominal energy of 510 MeV. However, the possibility of changing the energy of the particles in the rings by small amounts, of order of few times the width of the Φ resonance (≈5 MeV) around the nominal point is also taken into account.

1. Dipoles

The magnetic measurements on the four types of dipoles are presented in [3,4,5]. Being all the dipoles in each ring connected in series, the magnetic length of each one of the 16 magnets has been optimized in order to reach the correct field integral at a "conventional" current of 266.2 A, established during the measurements on the first prototype, the "parallel ends short (PES)" magnet. The end caps of all the dipoles have been machined following the criterion that the particle trajectories calculated on the field maps are bent by the nominal bending angles (40.5° for the "short" dipoles, 49.5° for the "long" ones) at an energy of 511.8 MeV under an excitation current of 266.2 A. Scaling the field around the operating point, the current required in the common loop to reach the nominal energy of 510 MeV is 264.8 A. The maximum current delivered by the main power supply is 750 A.

As discussed in [5], this condition is not satisfied exactly, and the correction windings should be used, although at a less than 10% of their maximum current, in order to avoid closed orbit distortions up to half a milliradian per magnet. These backleg windings are powered by bipolar power supplies capable of a maximum current of ±10 A and the response of the field at the magnet center is practically linear over this small range. It has been measured on the PES [3], SLS [4] and SLL [4] prototypes and found to be the same for the two types of short dipoles. Indicating with I_{BW} the current in the correction winding, the change in energy fixing the nominal bending angle and, correspondingly, the angular change at fixed energy are:

$$\Delta E_{PES,SLS} \ (MeV, \ @510 \ MeV) = 0.26 \ I_{BW} \ (A) \tag{1.1}$$

$$\Delta\alpha_{PES,SLS} \ (mrad, \ @510 \ MeV) = -0.36 \ I_{BW} \ (A)$$

The sign of the deflection angle is assumed positive towards the outside of the ring, as for all the correctors; the sign of I_{BW} is positive when the field generated by the corrector is in the same direction of the main field.

The effect of the correction winding has been found to be slightly larger in the SLL dipole prototype, and has not been measured in the PEL one. Following the result of the short magnets, it is assumed that the long dipoles have the same behaviour, namely:

$$\Delta E_{PEL,SLL} \ (MeV, \ @510 \ MeV) = 0.31 \ I_{BW} \ (A) \tag{1.2}$$

$$\Delta\alpha_{PEL,SLL} \ (mrad, \ @510 \ MeV) = -0.53 \ I_{BW} \ (A)$$

Table I shows the correction currents required to reach the correct deflection angles in the dipoles at 510 MeV. A positive sign of the current means that the field created by the corrector is in the same direction of the main field in the dipole.

Table I - Dipole correctors current @ 510 MeV

Name	Type	Serial#	I$_{BW}$ (A)
DHREL101	PEL	4	-0.17
DHSEL102	SLL	1	0.62
DHSES101	SLS	3	0.05
DHRES102	PES	4	0.00
DHRES201	PES	1	0.00
DHSES202	SLS	2	0.50
DHSEL201	SLL	3	-0.15
DHREL202	PEL	1	0.26
DHRPL101	PEL	3	0.08
DHSPL102	SLL	2	0.54
DHSPS101	SLS	1	-0.17
DHRPS102	PES	2	0.35
DHRPS201	PES	3	-0.12
DHSPS202	SLS	4	-0.08
DHSPL201	SLL	4	0.39
DHRPL202	PEL	2	0.12

The possibility of correcting the differences between the field integrals at beam energies different from the nominal one in the different kinds of dipoles by means of the correction windings is discussed in [3,4]. In order to establish a rule to change the beam energy around the nominal operation point (from, say, 490 to 530 MeV), we assume that over this small range the field integrals over the trajectory followed by the particles are proportional to the field measured at the magnet center, and that the calibration factors in (1.1) and (1.2) do not change. By means of a quadratic interpolation of the excitation curves around the nominal operating point, the relations between the beam energy and the current in the main dipole loops can be expressed as:

$$E \text{ (MeV)} = -5.0994 \times 10^{-3} \, I^2(A) + 4.0253 \, I(A) - 198.39$$

$$I(A) = 2.1972 \times 10^{-3} \, E^2(\text{MeV}) - 1.4826 \, E(\text{MeV}) + 449.45 \qquad (1.3)$$

$$490 \leq E(\text{MeV}) \leq 530 \qquad 250.5 \leq I(A) \leq 280.9$$

2. Wigglers

The 8 wigglers of the Main Rings have been measured at the same excitation current of 711.9 A in the main poles and 562.0 A in the terminal ones, corresponding to a maximum field of ±1.80 T. The main poles windings of the 4 wigglers in each ring are powered in series, while each wiggler has its power supply for the terminal poles, in order to compensate small differences in the integrated field. The measurements on the prototype and on the series production magnets are described in [6,7].

The sensitivity of the overall field integral, measured along the wiggler axis, to the current in the terminal poles winding is given by [7]:

$$\Delta\!\int\!Bds \text{ (Gm)} = -1.38 \ \Delta I_{TP} \text{ (A)} \qquad (2.1)$$

$$\Delta\alpha(\text{mrad}, @510 \text{ MeV}, 1.8\text{T}) = 8.1\times10^{-2} \ \Delta I_{TP} \text{ (A)}$$

Equation (2.1) indicates that increasing the current in the terminal poles with respect to the nominal value of 562.0 A gives a negative overall field integral and a positive beam deflection (towards the outside of the ring). Table II shows the current in the terminal poles required to compensate each wiggler as described in [7].

Table II - Wiggler terminal poles current (I = 711.9 A in main poles)

Name	Serial #	I_{TP} (A)
WGLEL101	95989	570.9
WGLES101	95995	575.0
WGLES201	95993	571.0
WGLEL201	95996	572.0
WGLPL101	95991	579.7
WGLPS101	95990	582.0
WGLPS201	95994	557.3
WGLPL201	95992	566.6

As explained in [8], the field integral compensation on the wiggler axis is equivalent to the compensation on the beam trajectory, due to the displacement of the wiggler axis with respect to the ideal trajectory in the straight section.

The compensation at different maximum fields has been studied only on the prototype [6]. At a maximum field of 1.2 T, obtained with 251.8 A in the main poles, the compensating current in the terminal poles is 218.0 A and the sensitivity is given by:

$$\Delta\!\int\!Bds \text{ (Gm)} = -4.92 \ \Delta I_{TP} \text{ (A)} \qquad (2.2)$$

$$\Delta\alpha(\text{mrad}, @510 \text{ MeV}, 1.2\text{T}) = 0.29 \ \Delta I_{TP} \text{ (A)}$$

The maximum field of 1.5 T is reached with 382.6 A in the main winding and 320.2 A in the terminal poles. The sensitivity is:

$$\Delta\!\int\!Bds \text{ (Gm)} = -3.14 \ \Delta I_{TP} \text{ (A)} \qquad (2.3)$$

$$\Delta\alpha(\text{mrad}, @510 \text{ MeV}, 1.5\text{T}) = 0.18 \ \Delta I_{TP} \text{ (A)}$$

In order to fit the behaviour of the maximum field (T), measured at the center of the wiggler, versus the current in the main pole winding (A, with the terminal poles off) it is convenient to separate the available current range into a low current part, where the field is linear, and a high current one, where a polynomial is a good approximation:

$$I \le 220 \text{ A} \qquad\qquad B(T) = 5.0605 \ 10^{-3} \ I \ (A) \qquad\qquad (2.4)$$

$$I \ge 220 \text{ A} \quad B(T) = -1.5199 \ 10^{-11} \ I^4 + 3.6814 \ 10^{-8} \ I^3 - 3.3272 \ 10^{-5} \ I^2 + 1.4107 \ 10^{-2} \ I - 0.73631$$

It is also useful to invert (2.4) to obtain the current as a function of the maximum field:

$$B \le 1.0 \text{ T} \qquad\qquad I(A) = 1.976 \ 10^2 \ B(T) \qquad\qquad (2.5)$$

$$B \ge 1.0 \text{ T} \quad I \ (A) = 4.7434 \ 10^2 \ B^3 - 1.1659 \ 10^3 \ B^2 + 1.0238 \ 10^3 \ B - 1.3464 \ 10^2$$

The current in the terminal poles needed to compensate the wiggler at any current in the main poles should be found by a direct measurement with the stored beam switching on a single wiggler at a time and measuring the closed orbit distortion as a function of the terminal poles excitation. The maximum current delivered by the power supply of both the main winding and terminal poles one is 750 A.

3. Splitters

The measurements on the 4 splitter magnets are described in [9,10]. The field inside the two gaps is generated by coils powered by independent power supplies. The measurements have been performed with the coils in series and it has been found that the differences between the absolute values of the field in the right and left gap of each magnet are negligible. The differences between the fields in the 4 splitters can be neglected as well. The field at the gap center is linear in the excitation current with a maximum current of 750 A from the power supply.

By tracking the particles in the measured field along the magnet [9], the relation between the excitation current and the energy of the particles performing the nominal deflection (8.75° for a crossing angle of 12.5 mrad) has been found to be:

$$E \ (MeV) = 1.1698 \ I \ (A) \qquad\qquad (3.2)$$

$$I \ (A) = 0.8548 \ E \ (MeV)$$

and therefore the nominal current on the DAY-ONE operating point is 436.0 A.

The angle at a given energy is:

$$\alpha \ (mrad) = 178.63 \ I \ (A)/E(MeV) \qquad\qquad (3.2)$$

$$I \ (A) = 5.5977 \ 10^{-3} \ \alpha \ (mrad) \ E \ (MeV)$$

Table III shows the correspondence between the serial numbers of the magnets and their position in the rings.

Table III - Splitters

Name	Serial #
SPLI1001	2
SPLI1002	1
SPLI2001	3
SPLI2002	4

4. Solenoid compensators

The solenoid compensators will not be used during the commissioning phase of the DAY-ONE structure. We include here the available data for sake of completeness only. The magnetic measurement on the solenoid compensators have been performed by the builder (OXFORD Instruments). From their results the integrated longitudinal field is linear and given by:

$$\int Bds \, (Tm) = 0.01343 \, I \, (A) - 0.087 \qquad (4.1)$$

$$I \, (A) = 74.46 \int Bds \, (Tm) + 6.48$$

The position of the single magnets is shown in Table IV.

Table IV - Solenoid compensators

Name	Serial #
SOLI1001	1
SOLI1002	2
SOLI2001	3
SOLI2002	4

5. Large aperture quadrupoles

The 8 large aperture quadrupoles described in [11,12] are used in the interaction regions of the DAY-ONE lattice. Also in this case there is saturation at high current. It is convenient to give an expression for the quadrupole strength K_Q related to the integrated gradient through the relation:

$$K_Q L_Q = 299.79 \qquad (5.1)$$

where L_Q is the nominal quadrupole length (**0.38** m) and $G = \partial B_y/\partial x = \partial B_x/\partial y$ its gradient.

In the following the absolute value is used for the current and quadrupole strength.

The sign of the strength K_Q is positive for a quadrupole focusing in the horizontal plane, which has a vertical field component in the horizontal plane in the same direction of the bending magnets on the external side of the ring, in the opposite one on the inside.

For the large aperture quadrupoles the fit is given by:

$I \leq 380$ A $\qquad |K_Q| (m^{-2}) = (3.9786 |I| (A) + 2.72)/E (MeV)$ $\qquad$ (5.2)

$I \geq 380$ A $\qquad |K_Q| (m^{-2}) = (-3.3801\ 10^{-3}\ I^2 + 6.299\ |I| -390.92)/E$

$|K_Q| E \leq 1547\ m^{-2}$ MeV $\qquad |I| (A) = 0.2516 |K_Q| E - 0.683$ $\qquad$ (5.3)

$|K_Q| E \geq 1547\ m^{-2}$ MeV $\qquad |I| (A) = 1.3325\ 10^{-4} (K_Q E)^2 - 0.15895 |K_Q| E + 315.5$

The maximum current is 585 A. Table V shows the correspondence between the serial numbers of the magnets and their position in the ring.

Table V - Large aperture quadrupoles

Name	Serial #	Name	Serial #
QUAI1001	3	QUAI2001	5
QUAI1002	8	QUAI2002	4
QUAI1006	6	QUAI2006	1
QUAI1007	7	QUAI2007	2

6. Large quadrupoles

Among the 28 large quadrupoles described in [13,14,15], 24 are placed in the achromats of the DAΦNE Main Rings, and the last four in the straight sections of the short arcs downstream the splitters near the KLOE interaction region to accommodate the large cross section vacuum chamber required by the tagging detector of the γ-γ experiment. Their nominal length is **0.29** m.

With the same conventions of Section 5, the fit of the quadrupole strength is:

$I \leq 123$ A $\qquad |K_Q| (m^{-2}) = (16.963 |I| (A) + 5.62)/E (MeV)$ $\qquad$ (6.1)

$I \geq 123$ A $\qquad |K_Q| (m^{-2}) = (-6.636\ 10^{-2}\ I^2 + 32.641\ |I| - 918.72) /E (MeV)$

$|K_Q| E \leq 2224\ m^{-2}$ MeV $\qquad |I| (A) = 0.0590 |K_Q| E - 0.360$ $\qquad$ (6.2)

$|K_Q| E \geq 2224\ m^{-2}$ MeV $\qquad I (A) = 4.091\ 10^{-5} (|K_Q| E)^2 - 0.1218 |K_Q| E + 199.3$

This type of quadrupoles are in the linear region for $|K_Q| < 4.16$ m^{-2} @ 510 MeV. The maximum current is 175 A.

Table VI - Large quadrupoles @ 510 MeV (DAY-ONE)

Name	Serial #	Name	Serial #
QUAEL105	22	QUAPL105	6
QUAEL106	18	QUAPL106	21
QUAEL107	24	QUAPL107	26
QUAES101	23	QUAPS101	8
QUAES102	5	QUAPS102	3
QUAES104	11	QUAPS104	9
QUAES105	7	QUAPS105	16
QUAES106	25	QUAPS106	1
QUAES204	27	QUAPS204	10
QUAES205	2	QUAPS205	12
QUAES206	4	QUAPS206	20
QUAEL204	13	QUAPL204	15
QUAEL205	17	QUAPL205	19
QUAEL206	0 (prototype)	QUAPL206	14

7. Small quadrupoles

The magnetic measurements on the 60 small quadrupoles used in the straight sections of the Main rings where the vacuum chamber diameter is less than 10 cm are presented in [16,17,18]. The nominal magnetic length of these magnets is 0.3 m and the maximum operating current is 585 A. 56 such quadrupoles are used in the DAY-ONE lattice.

With the same conventions of Section 5:

$I \leq 304$ A $\qquad\qquad$ $|K_Q|$ (m^{-2}) = (9.1277 |I| (A) + 4.53)/E (MeV) $\qquad$ (7.1)

$I \geq 304$ A $\qquad\qquad$ $|K_Q|$ (m^{-2}) = (-9.849 10^{-3} I^2 + 14.719 |I| -784.97)/E (MeV)

$|K_Q|$ E ≤ 3200 m^{-2} MeV $\qquad$ |I| (A) = 0.10956 $|K_Q|$ E - 0.496 $\qquad$ (7.2)

$|K_Q|$ E ≥ 3200 m^{-2} MeV $\quad$ I (A) = 3.8109 10^{-5} ($|K_Q|$ E)^2 - 0.10398 $|K_Q|$ E + 292.60

The strengths are in the linear region for $|K_Q| < 5.3$ m^{-2} @ 510 MeV.

Table VII - Small quadrupoles

Name	Serial #	Name	Serial #
QUAEL101	26	QUAPL101	32
QUAEL102	37	QUAPL102	12
QUAEL103	34	QUAPL103	11
QUAEL104	2	QUAPL104	38
QUAEL108	23	QUAPL108	3
QUAEL109	49	QUAPL109	15
QUAEL110	35	QUAPL110	27
QUAI1003	4		
QUAI1004	41		
QUAI1005	53		
QUAES103	60	QUAPS103	17
QUAES107	42	QUAPS107	25
QUAES108	9	QUAPS108	43
QUAES109	19	QUAPS109	33
QUAES110	48	QUAPS110	46
QUAES201	47	QUAPS201	57
QUAES202	31	QUAPS202	30
QUAES203	10	QUAPS203	56
QUAES207	29	QUAPS207	1
QUAES208	14	QUAPS208	51
QUAES209	16	QUAPS209	24
QUAI2003	59		
QUAI2004	54		
QUAI2005	28		
QUAEL201	40	QUAPL201	6
QUAEL202	7	QUAPL202	8
QUAEL203	52	QUAPL203	5
QUAEL207	36	QUAPL207	22
QUAEL208	50	QUAPL208	18
QUAEL209	13	QUAPL209	55
QUAEL210	39	QUAPL210	45

8. Large sextupoles

Among the 18 large sextupoles described in [15,19,20], 16 are placed in the achromats of the DAΦNE Main Rings, and the last two in the straight sections of the short arcs downstream the splitters near the KLOE interaction region to accommodate the large cross section vacuum chamber required by the tagging detector of the γ-γ experiment. Their nominal length is 0.15 m.

The integrated sextupole gradient, defined as the second derivative of the vertical field component along the horizontal direction, is linear up to an excitation current of 150A:

$$I \leq 150 \text{ A} \qquad |K_S|L_S \ (m^{-2}) = (51.177 \ |I| + 49.34)/E(MeV) \qquad (8.1)$$

$$I \geq 150 \text{ A} \qquad |K_S|L_S \ (m^{-2}) = (-0.15573 \ I^2 + 103.08 \ |I| - 4232.2)/E(MeV)$$

$$|K_S|L_S \ E \leq 7500 \ m^{-2} \ MeV \qquad |I| \ (A) = 1.954 \ 10^{-2} \ (|K_S|L_S \ E) - 0.9641 \qquad (8.2)$$

$$|K_S|L_S \ E \geq 7500 \ m^{-2} \ MeV \qquad |I| \ (A) = 8.5958 \ 10^{-10}(|K_S|L_S \ E)^3 -$$

$$- 2.3197 \times 10^{-5} \ (|K_S|L_S \ E)^2 + 0.22822 \ (|K_S|L_S \ E) - 623.87$$

Table VII shows the positions of the sextupoles, the integrated sextupole strength $K_S L_S$ defined by:

$$|K_S|L_S \ (m^{-2}) \ = 299.79 \ \frac{\left|\int Sds\right|(T/m)}{E(MeV)} \qquad (8.3)$$

the integrated sextupole gradient and the excitation current for each sextupole. A sextupole with negative strength, located where the horizontal dispersion is positive, compensates the horizontal chromaticity. The vertical field component has the same direction as the bending magnets on both sides of the sextupole axis in the horizontal plane. The large sextupoles are in the linear region for $|K_S| \ L_S \leq 14.7 \ m^{-2}$ @510 MeV. The maximum operating current is 250 A.

Table VIII - Large sextupoles

Name	Serial #	Name	Serial #
SXPEL102	12	SXPPL102	7
SXPEL103	16	SXPPL103	2
SXPES101	9	SXPPS101	8
SXPES102	11	SXPPS102	0 (prototype)
SXPES103	10	SXPPS103	5
SXPES202	3	SXPPS202	13
SXPES203	1	SXPPS203	15
SXPEL202	6	SXPPL202	17
SXPEL203	4	SXPPL203	14

9. Small sextupoles

The results of the measurements on the small sextupoles are described in [18,21,22]. These magnets are used in the straight sections of the Main rings where the vacuum chamber diameter is less than 10 cm and their nominal magnetic length is 0.1 m. The maximum current is 336 A.

The behaviour of the integrated sextupole strength is linear over the whole operating range:

$$|K_S|L_S \ (m^{-2}) = (19.741 \ |I| + 32.80)/E(MeV) \tag{9.1}$$

$$|I| \ (A) = 5.0656 \ 10^{-2} \ (|K_S|L_S \ E) - 1.661$$

Table XI shows the positions of the sextupoles, the sextupole strength $K_S \ L_S \ (m^{-2})$, the integrated sextupole gradient and the excitation current for the small sextupoles.

<p align="center">Table IX - Small sextupoles</p>

Name	Serial #	Name	Serial #
SXPEL101	1	SXPPL101	6
SXPEL104	8	SXPPL104	12
SXPES104	7	SXPPS104	2
SXPES201	11	SXPPS201	5
SXPES204	14	SXPPS204	9
SXPEL201	13	SXPPL201	10
SXPEL204	3	SXPPL204	4

10. CHV + Skew quadrupole correctors

Each one of these 16 correctors is placed near a bending magnet in the Main Rings. They are used to correct the closed orbit errors both in the horizontal and vertical planes, and have an additional skew quadrupole winding in order to realize uncoupled transfer matrices from one interaction point to the other. The magnetic measurements are described in [23].

The correctors are in the linear regime even when all the three windings are excited at their maximum currents at the same time. The effects of the different windings add therefore linearly.

For the horizontal and vertical corrector windings the integrated field on the magnet axis is given by:

$$\int B_{X,Y} ds \ (Tm) = 5.771 \ 10^{-5} \ I_{CH,CV} \ (A) \tag{10.1}$$

where the maximum value of the excitation current for each winding is ±215 A. It is useful to express the bending power of the correctors in terms of the bending angle as a function of the current and beam energy:

$$\alpha_{X,Y} \ (mrad) = 17.3 \ I_{CH,CV} \ (A) / E \ (MeV) \tag{10.2}$$
$$I_{CH,CV} \ (A) = 5.78 \ 10^{-2} \ \alpha_{X,Y} \ (mrad) \ E \ (MeV)$$

The skew quadrupole winding can be excited up to 280 A. The integrated skew gradient is linear and given by:

$$\int \frac{\partial B_x}{\partial_x} \ ds = \int \frac{\partial B_y}{\partial_y} \ ds = 9.52 \times 10^{-4} \ I \ (A) \tag{10.3}$$

This integrated gradient contributes to the 4x4 betatron matrix element of the skew quadrupole as described in [24]. Table X shows the correspondence between the serial numbers of the correctors and their position in the rings.

Table X - CHV + Skewquad correctors

Name	Serial #	Name	Serial #
CHVEL103	15	CHVPL103	11
CHVEL106	12	CHVPL106	09
CHVES101	13	CHVPS101	10
CHVES104	01	CHVPS104	06
CHVES202	16	CHVPS202	03
CHVES205	08	CHVPS205	14
CHVEL201	02	CHVPL201	04
CHVEL204	07	CHVPL204	05

11. CHV Square correctors

The 14 square correctors [25] are used in the injection and RF straight sections. Also in this case the contributions of the horizontal and vertical correctors add linearly. From the magnetic measurements, the beam deflection as a function of the excitation current in each winding is given by:

$$\alpha_{X,Y} \text{ (mrad)} = 210 \ I_{CH,CV} \text{ (A) } / \text{ E (MeV)} \tag{11.1}$$
$$I_{CH,CV} \text{ (A)} = 4.76 \times 10^{-3} \ \alpha_{X,Y} \text{ (mrad) E (MeV)}$$

The maximum operating current is ± 10 A. The position of the square correctors is shown in Table XI.

Table XI - CHV Square correctors

Name	Serial #	Name	Serial #
CHVEL101	02	CHVPL101	12
CHVEL102	04	CHVPL102	09
CHVES105	13	CHVPS105	10
CHVES106	05	CHVPS106	03
CHVES201	14	CHVPS201	07
CHVEL205	06	CHVPL205	11
CHVEL206	08	CHVPL206	01

12. CHV Rectangular correctors

There are 16 CHV correctors of the rectangular type in the achromat straight sections between the dipoles, where the vacuum chamber has a variable shape, typically much larger in the horizontal direction than in the other straight sections in the arcs. For this reason these correctors have a rectangular shape and the deflecting power is different between the horizontal and vertical directions.

The contributions of the two windings add linearly and the magnetic measurements [26] yield the following calibrations:

$$\alpha_X \text{ (mrad)} = 186 \ I_{CH} \text{ (A)} / E \text{ (MeV)} \qquad (12.1)$$
$$I_{CH} \text{ (A)} = 5.38\text{x}10^{-3} \ \alpha_X \text{ (mrad) } E \text{ (MeV)}$$

$$\alpha_Y \text{ (mrad)} = 173 \ I_{CV} \text{ (A)} / E \text{ (MeV)} \qquad (12.2)$$
$$I_{CV} \text{ (A)} = 5.78\text{x}10^{-3} \ \alpha_Y \text{ (mrad) } E \text{ (MeV)}$$

The maximum operating current is ± 10 A. The names and serial numbers of these correctors are shown in Table XII.

Table XII - CHV Rectangular correctors

Name	Serial #	Name	Serial #
CHVEL104	10	CHVPL104	08
CHVEL105	11	CHVPL105	04
CHVES102	07	CHVPS102	03
CHVES103	06	CHVPS103	16
CHVES203	01	CHVPS203	09
CHVES204	13	CHVPS204	15
CHVEL202	14	CHVPL202	02
CHVEL203	05	CHVPL203	12

13. CHV "Lambertson" correctors

A couple of "Lambertson" correctors [27] is placed near each splitter magnet on the interaction region side. Also in this case the contributions of the horizontal and vertical windings add linearly and the calibrations are:

$$\alpha_X \text{ (mrad)} = 6.81 \ I_{CH} \text{ (A)} / E \text{ (MeV)} \qquad (13.1)$$
$$I_{CH} \text{ (A)} = 0.147 \ \alpha_X \text{ (mrad) } E \text{ (MeV)}$$

$$\alpha_Y \text{ (mrad)} = 16.1 \ I_{CV} \text{ (A)} / E \text{ (MeV)} \qquad (13.2)$$
$$I_{CV} \text{ (A)} = 6.21\text{x}10^{-2} \ \alpha_Y \text{ (mrad) } E \text{ (MeV)}$$

The horizontal corrector winding CH can be operated up to ± 215 A, the vertical one (CV) up to ± 150 A. The names and serial numbers of the "Lambertson" correctors are shown in Table XIII.

Table XIII - CHV "Lambertson" correctors

Name	Serial #	Name	Serial #
CHVEI101	07	CHVPI102	04
CHVEI102	01	CHVPI101	08
CHVEI201	06	CHVPI202	03
CHVEI202	05	CHVPI201	02

14. CHV "C" correctors

The horizontal/vertical "C" correctors [28] are placed downstream each splitter in order to allow the variation of the crossing angle at the interaction point. They act therefore as bending magnets in the horizontal plane when the crossing angle is different from the design value of 12.5 mrad. For this reason their conventional names do not begin with CHV as the other correctors. However, they have also a vertical corrector winding which is used to create e vertical orbit perturbation in the interaction region in order to separate the beams at the crossing point during the injection phase, and also to scan one beam with respect to the other in the vertical plane in order to find the optimum superposition. The calibrations for the two planes again independent from each other, are:

$$\alpha_X \text{ (mrad)} = 64.9 \ I_{CH} \text{ (A)} / E \text{ (MeV)} \tag{14.1}$$
$$I_{CH} \text{ (A)} = 1.54 \times 10^{-2} \ \alpha_X \text{ (mrad)} \ E \text{ (MeV)}$$

$$\alpha_Y \text{ (mrad)} = 43.5 \ I_{CV} \text{ (A)} / E \text{ (MeV)} \tag{14.2}$$
$$I_{CV} \text{ (A)} = 2.30 \times 10^{-2} \ \alpha_Y \text{ (mrad)} \ E \text{ (MeV)}$$

The maximum current in the CH winding is ±215 A, in the CV one ±150 A. The names and serial numbers of the correctors are shown in Table XIV.

Table XIV - "C" correctors

Name	Serial #	Name	Serial #
DHCEL101	03	DHCPL101	02
DHCES101	01	DHCPS101	04
DHCES201	05	DHCPS201	07
DHCEL201	08	DHCPL201	06

References

[1] M.E. Biagini, C. Biscari, S. Guiducci: "DAΦNE Main Rings lattice update", DAΦNE Technical Note L-22, 18/3/96.

[2] C. Biscari, F. Sgamma: "Coordinates of DAΦNE Main Rings magnetic elements", DAΦNE Technical Note ME-3, 6/6/95.

[3] B. Bolli, N. Ganlin, F. Iungo, F. Losciale, M. Modena, M. Paris, M. Preger, C. Sanelli, F. Sardone, F. Sgamma, M. Troiani: "The "short" dipoles of the DAΦNE Main Ring achromats", DAΦNE Technical Note MM-19, 2/8/1996.

[4] B. Bolli, N. Ganlin, F. Iungo, F. Losciale, M. Paris, M. Preger, C. Sanelli, F. Sardone, F. Sgamma, M. Troiani: "The 'long' dipoles of the DAΦNE Main Rings achromats", DAΦNE Technical Note MM-25, 21/5/1997.

[5] B. Bolli, N. Ganlin, F. Iungo, F. Losciale, M. Paris, M. Preger, C. Sanelli, F. Sardone, F. Sgamma, M. Troiani: "The dipoles of the DAΦNE Main Rings achromats", DAΦNE Technical Note MM-26, 22/5/1997.

[6] B. Bolli, F. Iungo, M. Modena, M. Preger, C. Sanelli, F. Sgamma, S. Vescovi: "Measurements on the Wiggler Magnet for the DAΦNE Main Ring", DAΦNE Technical Note M-4, 28/4/1994.

[7] B. Bolli, N. Ganlin, F. Iungo, F. Losciale, M. Preger, C. Sanelli, F. Sardone: "Magnetic measurements on the series production wigglers of the DAΦNE achromats", DAΦNE Technical Note MM-29, 30/6/1997.

[8] M. Bassetti, C. Biscari, M. Preger: "Optical characteristics of the DAΦNE wiggler", DAΦNE Technical Note G-27, 20/9/1994.

[9] C. Biscari, B. Bolli, N. Ganlin, F. Iungo, F. Losciale, M. Paris, M. Preger, C. Sanelli, F. Sardone, F. Sgamma, M. Troiani: "Measurements on TESLA splitter prototype for the DAΦNE Main Rings", DAΦNE Technical Note MM-20, 16/12/1996.

[10] B. Bolli, F. Iungo, F. Losciale, M. Paris, M. Preger, C. Sanelli, F. Sardone, F. Sgamma, M. Troiani: "Magnetic measurements on the four splitters of the DAΦNE interaction regions", DAΦNE Technical Note MM-28, 20/6/1997.

11 B. Bolli, N. Ganlin, F. Iungo, F. Losciale, M. Paris, M. Preger, C. Sanelli, F. Sardone, F. Sgamma, M. Troiani: "The large aperture quadrupole prototype for the DAΦNE interaction regions", DAΦNE Technical Note MM-22, 27/1/1997.

[12] B. Bolli, F. Iungo, F. Losciale, M. Paris, M. Preger, C. Sanelli, F. Sardone, F. Sgamma, M. Troiani: "Field quality and alignment of the large aperture quadrupoles of the DAΦNE Interaction Regions", DAΦNE Technical Note MM-30, 22/7/1997

[13] B. Bolli, N. Ganlin, F. Iungo, F. Losciale, M. Paris, M. Preger, C. Sanelli, F. Sardone, F. Sgamma, M. Troiani: "Misura delle caratteristiche magnetiche del quadrupolo prototipo per gli archi dei Main Rings", DAΦNE Technical Note MM-13 (in italian), 19/4/1996.

[14] B. Bolli, N. Ganlin, F. Iungo, F. Losciale, M. Preger, C. Sanelli, F. Sardone: "Field quality of the large quadrupoles for the DAΦNE Main Rings", DAΦNE Technical Note MM-24, 22/4/1997.

[15] B. Bolli, N. Ganlin, F. Iungo, F. Losciale, M. Paris, M. Preger, C. Sanelli, F. Sardone, F. Sgamma, M. Troiani: "Comparison of magnetic and mechanical center positions of the large quadrupoles and sextupoles in the DAΦNE Main Rings achromats", DAΦNE Technical Note MM-27, 23/5/1997.

[16] B. Bolli, F. Iungo, M. Modena, M. Preger, C. Sanelli, F. Sgamma, M. Troiani, S. Vescovi: "Measurements On Tesla Quadrupole Prototype for the DAΦNE Accumulator and Main Rings", DAΦNE Technical Note MM-4, 2/12/1994.

[17] B. Bolli, F. Iungo, F. Losciale, N. Ganlin, M. Preger, C. Sanelli, F. Sardone: "Field quality of the small quadrupoles for the DAΦNE Main Rings", DAΦNE Technical Note MM-10, 22/2/1996.

[18] B. Bolli, N. Ganlin, F. Iungo, F. Losciale, M. Paris, M. Preger, C. Sanelli, F. Sardone, F. Sgamma, M. Troiani: "Comparison of magnetic and mechanical center positions of small quadrupoles and sextupoles in the DAΦNE Main Rings", DAΦNE Technical Note MM-23, 19/3/1997.

[19] B. Bolli, N. Ganlin, F. Iungo, M. Paris, M. Preger, C. Sanelli, F. Sardone, F. Sgamma, M. Troiani: "Measurements on Ansaldo sextupole prototype for the DAΦNE Main Rings (Large sextupole)", DAΦNE Technical Note MM-12, 26/3/1996.

[20] B. Bolli, N. Ganlin, F. Iungo, F. Losciale, M. Preger, C. Sanelli, F. Sardone: "Magnetic measurements on the large sextupoles for the DAΦNE Main Rings achromats", DAΦNE Technical Note MM-21, 22/1/1997.

[21] B. Bolli, F. Iungo, M. Modena, M. Paris, M. Preger, C. Sanelli, F. Sardone, F. Sgamma, M. Troiani: "The DAΦNE accumulator sextupoles", DAΦNE Technical Note MM-6, 10/5/1995.

[22] B. Bolli, F. Iungo, F. Losciale, N. Ganlin, M. Preger, C. Sanelli, F. Sardone: "Field quality of the small sextupoles for the DAΦNE Main Rings", DAΦNE Technical Note MM-11, 6/3/1996.

[23] B. Bolli, N. Ganlin, F. Iungo, F. Losciale, M. Paris, M. Preger, C. Sanelli, F. Sardone, F. Sgamma, M. Troiani: "Measurements on SIGMA-PHI CHV+SkewQuad corrector prototype for the DAΦNE Main Rings", DAΦNE Technical Note MM-16, 8/6/1996.

[24] C. Biscari: "Correcting coils in low-β insertion quadrupoles", DAΦNE Technical Note IR-7, 18/1/1996.

[25] B. Bolli, N. Ganlin, F. Iungo, F. Losciale, M. Paris, M. Preger, C. Sanelli, F. Sardone, F. Sgamma, M. Troiani: "Measurements on SIGMA-PHI square corrector prototype for the DAΦNE Main Rings", DAΦNE Technical Note MM-14, 7/6/1996.

[26] B. Bolli, N. Ganlin, F. Iungo, F. Losciale, M. Paris, M. Preger, C. Sanelli, F. Sardone, F. Sgamma, M. Troiani: "Measurements on SIGMA-PHI rectangular corrector prototype for the DAΦNE Main Rings", DAΦNE Technical Note MM-15, 7/6/1996.

[27] B. Bolli, N. Ganlin, F. Iungo, F. Losciale, M. Paris, M. Preger, C. Sanelli, F. Sardone, F. Sgamma, M. Troiani: "Measurements on Tesla "Lambertson" corrector prototype for the DAΦNE Main Ring", DAΦNE Technical Note MM-18, 3/7/1996.

[28] B. Bolli, N. Ganlin, F. Iungo, M. Paris, M. Preger, C. Sanelli, F. Sardone, F. Sgamma, M. Troiani: "Measurements on Tesla "C" corrector prototype for the DAΦNE Main Rings", DAΦNE Technical Note MM-17, 28/6/1996.
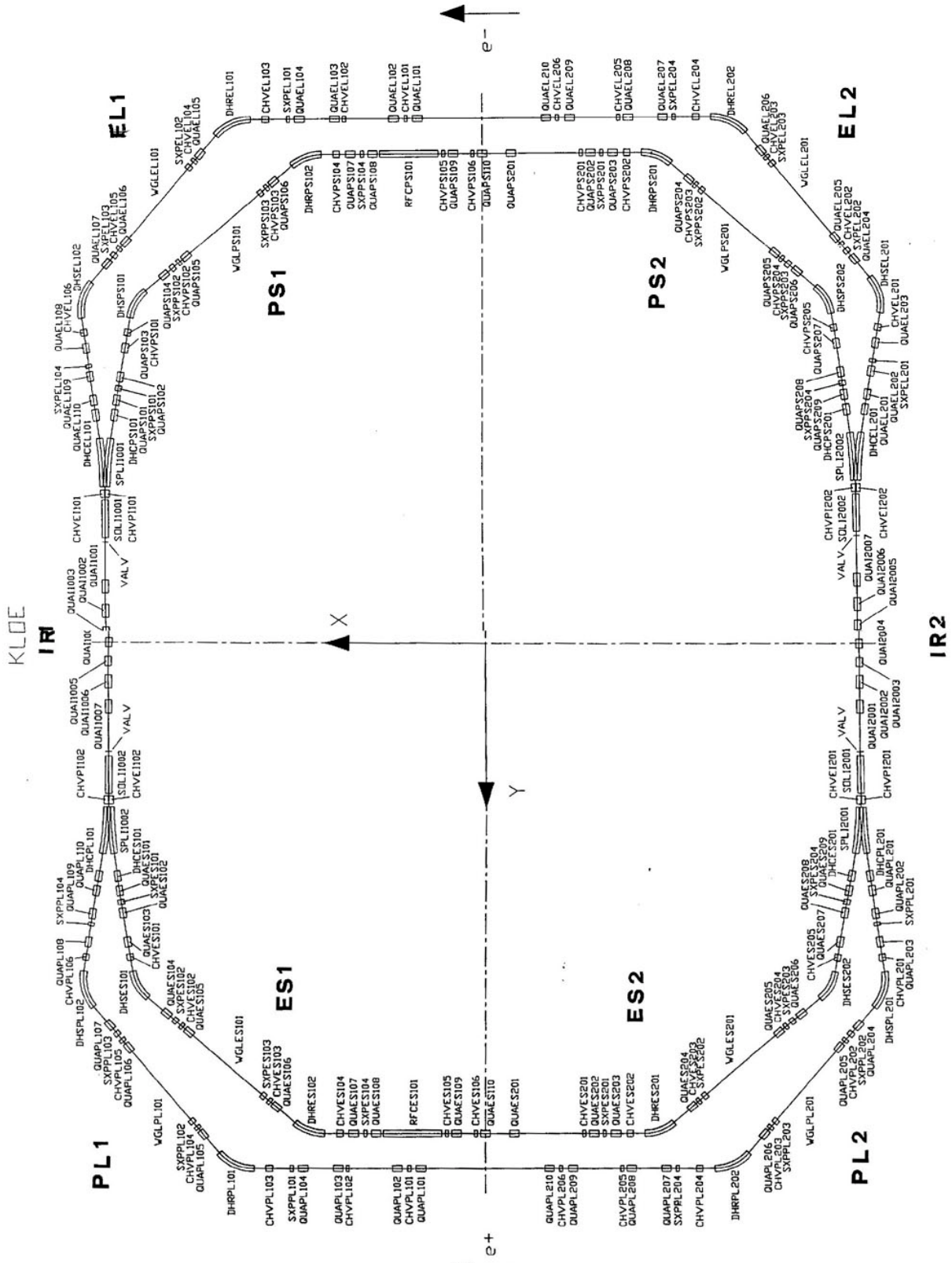
Figure 1